International Journal of Civil Engineering

Structure - Steel

# Finite element based fatigue assessment of corrugated steel web beams in highway bridges

**Z.Y. Wang[1,*], Q.Y. Wang[2], R.J. Jiang[3]**

Received: May 2013, Revised: September 2014, Accepted: April 2015

***Abstract***

*This paper presents a finite element analysis and its related experimental test of corrugated steel web beams subjected to fatigue loading. A particular focus in this study was set on the fatigue failure arising from web-to-flange welded joints of corrugated steel web beams. Using ANSYS and FE-SAFE software packages, a detailed three-dimensional finite element model which explicitly includes the geometry of the web-to-flange welds along the corrugated web was developed to simulate the test corrugated web beams. The finite element model is verified by comparing with related fatigue experimental test results. The effective notch stress approach was also applied to analyse the web-to-flange welded joint replicating the local critical region in the corrugated web beam. The fatigue strength of the web-to-flange welded joint was evaluated and compared numerically by considering the stress distribution at potential fatigue crack initiation location. The fatigue life of the corrugated steel web beam was assessed numerically by incorporating material S-N relation and employing fracture mechanics approach. The comparison with fatigue test results show that it is possible to expect the fatigue crack failure arising at the weld root or weld toe corresponding to the sections with reference angle using the effective notch stress analysis. The range of these predictions was evaluated by comparing with fatigue test results with good accuracy and can be considered between AASHTO fatigue categories B and B'. The parametric notch stress analysis incorporating the influences of corrugation angle was performed and demonstrates it is possible to expect the fatigue crack failure arising at the weld root or weld toe. Finally, a practical solution for possible fatigue life enhancement of such structure is suggested by decreasing corrugation angle or smoothing the intersection geometry of the corrugated web together with moderate increase of the flange thickness.*

***Keywords:*** *Corrugated steel web beam, Stress concentration, Life prediction, Fatigue, Finite element analysis.*

## 1. Introduction

Corrugated steel web plate has a promising application in configuring large span highway bridge girders. Its inherent high out-of-plane stiffness reduces the web buckling problem and saves transverse stiffeners for reinforcement which in turn decreases fabrication costs in steel plate girders. On the other hand, the so-called 'accordion effect' of corrugated web plates eases the introduction of prestress into the concrete flanges in prestressed concrete box girders [1]. Also, the girders with corrugated steel webs have less weight in contrast to those with concrete webs in practice. An exemplified application is the Weihe highway bridge with span 47+52+47m in China completed in the year of 2010, as shown in Fig.1(a)-(b). Dual six-lane and vehicle driving speed at 120km/h was considered in its structural design..The continuous box girder in this bridge consists of a single box three-cell cross-section. The corrugated webs are welded to the flange of steel beams. Meanwhile, the steel beams are connected with concrete deck with T-Perfobond shear connectors, as shown in Fig.1(c) [2,3].

During service life, bridges are subjected to repeated loadings causing fatigue which poses a major problem limiting the loading carrying capacity. The effect of fatigue on the failure of welded steel bridges has been well recognized in the literature [4]. Recently, the fatigue vulnerability of web-to-flange welded joints connecting corrugated steel web and flange plate has been detected in several fatigue tests of bare corrugated steel web beams [5-11]. The fatigue strength of the corrugated web beams is reduced as the web-to-flange welded joints suffer from defects resulting in the notch effect and surface cracks. Also, an important issue concerning concrete-steel composite girder is that the fatigue cracks even appear at the web-to-flange welded joint connecting corrugated web and steel beam flange plate anchored in concrete [12]. Therefore, it is necessary to ensure that the web-to-flange

** Corresponding author: zywang@scu.edu.cn*
*1 Associate Professor, Department of Civil Engineering, Institute of Architecture and Environment, Sichuan University, Chengdu, PR China*
*2 Professor, Department of Mechanics, Institute of Architecture and Environment, Sichuan University, Chengdu, PR China*
*3 Professorate Senior Engineer, Shenzhen Municipal Design & Research Institute Co., Ltd, Shenzhen, PR China*



[ DOI: 10.22068/IJCE.13.4.419 ]

welded joints in the corrugated steel web beams possess adequate fatigue strength capacity as a basic issue for such prestressed concrete girders with corrugated steel webs during service life.

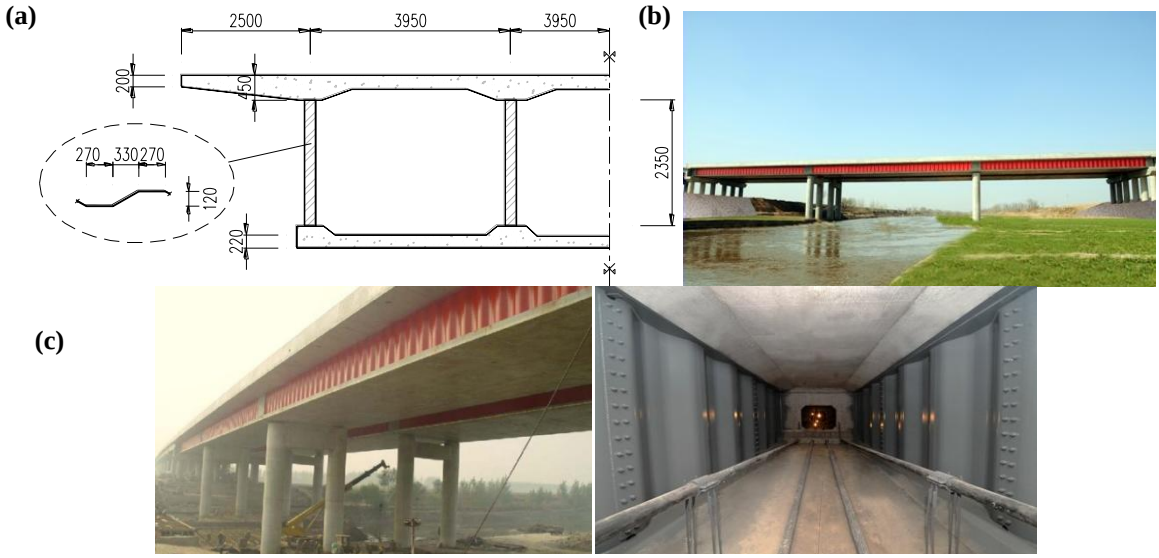


**Fig.1** Exemplified bridge structure with corrugated webs completed in China, 2010: (a) cross-section of a box girder with corrugated webs (dimensions in mm), (b) overview of the bridge, (c) details of corrugated steel webs jointing flange plates [2,3]

The fatigue behaviour of the corrugated steel web beam is complicated owing to the geometric configuration of the corrugated web plate. As such, the stress distribution at the location near the web-to-flange welded joints is complex and depends on the influencing factors including: corrugation angle, flange thickness and weld defects. Compared with experimental study limited by instrumentation, the development of finite elements has provided an attractive means to explore wide range of these related variables. However, the use of this method for the analysis of corrugated web beams is frequently lacking as reported in the literature. Ibrahim et al. [5] conducted a finite element modelling in studying the failure mode and stress concentration at the base of the fold line of the corrugated web beams. Unfortunately, few attempts were made to explicitly incorporate the stiffness of the web-to-flange welded joints in the three-dimensional model and take into account its related variables for fatigue life prediction which can be useful for the design of such structures.

As a follow-up study of the fatigue tests carried by the authors [9-11], the aim of this study was to further the understanding of the fatigue behaviour and provide possible solutions for fatigue life enhancement of the corrugated steel web beams. Fig. 2 illustrates a general fatigue analytical & design procedure implemented in current study. In this procedure, the source finite element model incorporating the geometric and loading data related to initial design is analysed first, and then the resultant data is exported for following fatigue stress-life analysis. The analytical results at each stage are compared with fatigue experimental tests and assist improvement & redesign.

This paper presents a detailed finite element modelling of the corrugated web beam with the aid of ANSYS 12.1. The basic material mechanical properties were obtained from experimental tensile tests. The stress concentration & distribution characteristics of corrugated web beams were analysed using finite element analysis. The effective notch stress approach was applied to evaluate the fatigue strength of the web-to-flange welded joints which are expected to suffer fatigue cracks initiation at the weld root or the weld toe. Afterwards, the fatigue life analysis was performed via FE-SAFE 6.2. The fatigue loading condition of the experimental tests was simulated in this analysis. An estimated *S-N* relation for the material was introduced with the consideration of the fatigue strength modifying factors. Also, the fracture mechanics approach was adopted for further comparison. Based on the analytical results, comments are given for the influencing parameters regarding the fatigue lives of corrugated steel web beams. The corresponding methods for fatigue life enhancement are also discussed.

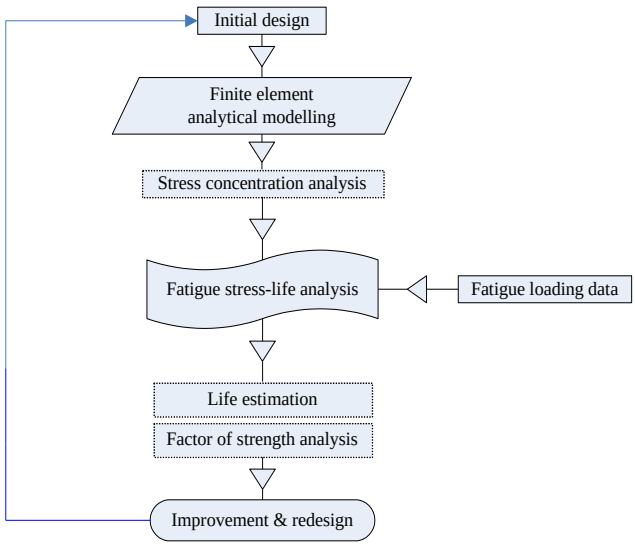


**Fig. 2** Flow chart in numerical fatigue life prediction and design



[ DOI: 10.22068/IJCE.13.4.419 ]

## 2. Description of Fatigue Tests

In the context of the current experimental study, several specimens were tested at the Sichuan Provincial Key Laboratory of Failure Mechanics and Engineering Disaster Prevention & Mitigation of Sichuan University [9] to analyse the fatigue behaviour of the corrugated steel web girders. The fatigue behaviour of corrugated steel web beam, configurationally comparable to the component of interest in the highway bridges, has been determined by a typical three-point bending test in this study as shown in Fig. 3. The test beam is supported at points A and B and the combined bending moment ($M_b$) and shearing force ($V_b$) are expected at the mid-span (point B of Fig. 3). Assuming the failure is produced by the load of $F_b$, it is evident that the maximum $M_b$ and $V_b$ can be derived as follows:

$$\begin{cases} M_b = \dfrac{F_b L_b}{4} \\ V_b = \dfrac{F_b}{2} \end{cases} \quad (1)$$

where, $L_b$ is the beam span.

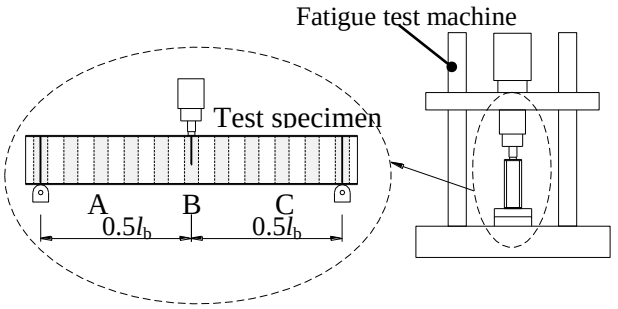


**Fig. 3** Schematic of a three point fatigue loading test

The dimension and configuration of the test corrugated web beam are illustrated in Fig. 4. The corrugation angle, α, which is defined as the angle of the inclined fold to the longitudinal direction of the beam, was considered as 30º and 45º for following comparison in the test. The test beam was stiffened at the loading and support points with transverse stiffeners at the mid-width of the inclined folds of corrugated web to avoid local failure at these points in loading. The fatigue loading was applied and controlled using a form of sinusoidal wave with constant frequency of 3Hz. The repeated loading with minimum and maximum applied loads at 8kN and 80kN respectively, as shown in Fig. 5, continued until the fatigue failure occurred. In this case, failure is defined as the crack initiating in the vicinity of the weld toe spreads laterally across the plate and reaches the flange tip. Monotonic loading and full cycle reading were conducted when the repetitive loading was applied at following intervals: 150,000th cycle; 600,000th cycle; 1,000,000th cycle; 2,000,000th cycle. The vertical deflection of test beams at mid-span was measured using Linear Variable Differential Transformers (LVDTs). Also, the strains were recorded by four single element strain gauges (SG) placed transversely on the top surface of tension flange (connecting corrugated web) near the centre of span. During the fatigue test, the fatigue cracks initiation was detected after 1,500,000 cycles and the fatigue failure took place at the web-to-flange welded joint where the longitudinal fold and the inclined fold of the corrugated web intersects as shown in Fig. 6. Also, there were some fatigue crack initiations along the web-to-flange fillet weld connecting the inclined fold of the corrugated web. In this test specimen with the corrugation angle of 45º, the fatigue cracks initiation was detected after 1,500,000 cycles and the final fatigue life was about 3,200,700 cycles.

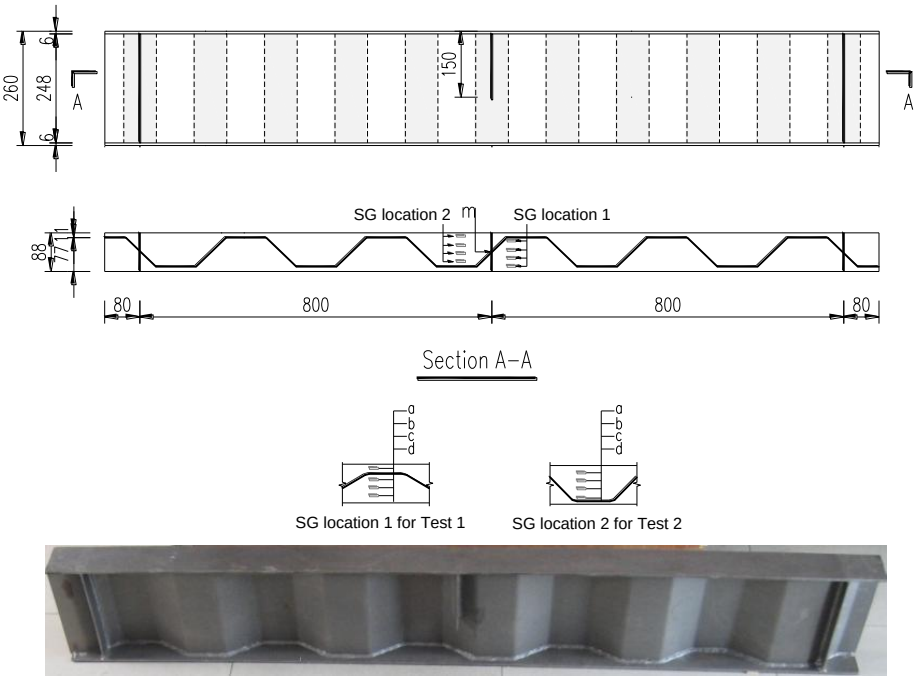


**Fig. 4** Geometric illustration of a test steel corrugated web beam



[ DOI: 10.22068/IJCE.13.4.419 ]

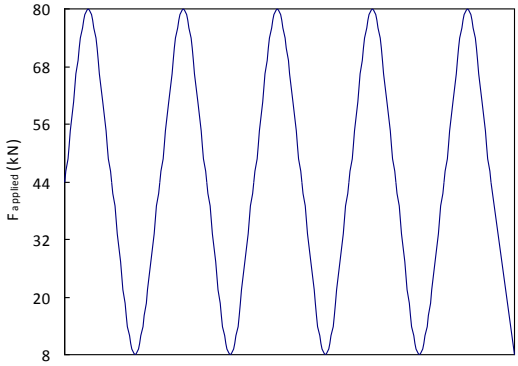


**Fig. 5** Loading procedure in the fatigue test

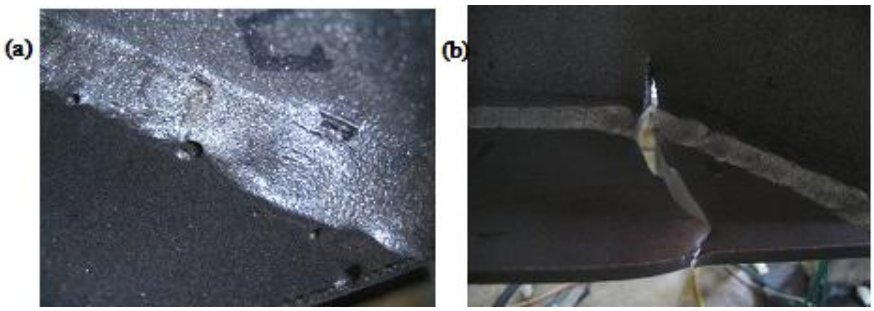


**Fig. 6** Photograph of fatigue crack initiation after 1500000 cycles and failure after 3200700 cycles

## 3. Finite Element Analytical Model

In the corrugated steel web beam, the corrugated web and flange plates are joined with fillet welds through $CO_2$ shielded semiautomatic Gas Metal Arc Welding (GMAW). To explicitly include the stiffness of the fillet welds in the analysis, element assemblies representing fillet welds were created in the model connecting the corrugated web and the flange plate. The contour lines of fillet weld toe and corrugated web are parallel along the longitudinal fold and inclined fold of the corrugated web. Adjacent to the intersection of aforementioned two folds of the corrugated web, it was assumed that these contour lines related to the internal and external corner of the corrugated web are tracked by inscribed circles with an identical circle centre. The basic geometry of the model was built in AutoCAD and then incorporated into ANSYS 12.1 preprocessing environment. The three dimensional finite element model of the corrugated steel web beam is shown in Fig. 7. The models were created using SOLID185 element, which is defined by eight nodes having three degrees of freedom at each node. This element avoids the problem deriving from the high order solid element degeneration to the shape of pyramid, for which the due consideration should be given so as to minimize the stress gradients. In the vicinity of the web-to-flange fillet weld regions, relative fine mesh was used to allow more accurate stress distribution transferred by external force.

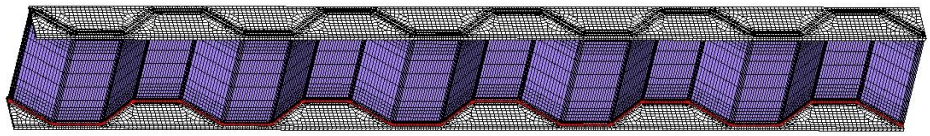

**Fig. 7** Finite element model of the corrugated web beam

The steel used in the experiment conforms to Q345 steel of the Chinese national standard GB/T700. The welding wire material (Type: ER50-6) and fillet welds meet the requirement of the Chinese national standards GB50017-2003 [13] and GB/T8110-2008 [14]. The chemical composition and mechanical properties of steel and welding wire materials are listed in Table 1. In the structural stress analysis, the mechanical properties of material were chosen according to experiment data. The ideal bilinear stress-strain relationship was considered for material model, as shown in Fig. 8. The initial slope was taken as the elastic modulus ($E_s$) and the Poisson's ratio was assumed as 0.3. The post yield modulus ($E_t$) is set at 1.5% of $E_s$. The strain ($\varepsilon_s$) corresponding to two ascent stages of the curve can be expressed as:

$$\varepsilon_s = \begin{cases} \dfrac{\sigma_s}{E_s} & 0<\varepsilon_s \le \varepsilon_y \\ \varepsilon_y + \dfrac{\sigma_s - \sigma_y}{E_t} & \varepsilon_s \ge \varepsilon_y \end{cases} \quad (2)$$

where, $\sigma_y$ and $\varepsilon_y$ are yield stress and strain respectively.



[ DOI: 10.22068/IJCE.13.4.419 ]

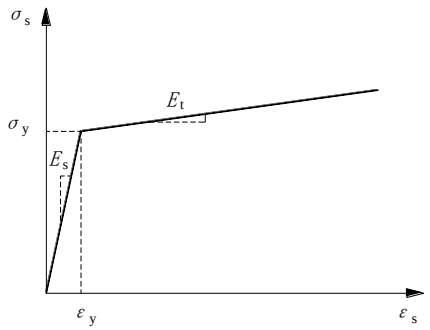


**Fig. 8** Assumed stress-strain relationship for structural steel

**Table 1** Chemical composition and mechanical properties of steel and welding wire materials

| Type | Chemical composition (%) | | | | | Mechanical properties | | |
|---|---|---|---|---|---|---|---|---|
| | C | $S_i$ | $M_n$ | P | S | Yield stress (MPa) | Ultimate stress (MPa) | Elongation (%) |
| Q345 | 0.16 | 0.33 | 1.36 | 0.035 | 0.022 | 400 | 555 | 33 |
| ER50-6 | 0.06-0.15 | 0.8-1.15 | 1.4-1.85 | <0.025 | <0.035 | >420 | 490-660 | ⩾22 |

The constraints and loading settings used in the finite element were the same as those in the fatigue test. For instance, the smooth beam surfaces at support and loading points were ensured to provide simply supported conditions and avoid any eccentricity in loading. Lateral braces were also installed at the support and loading point to avoid lateral distortion failure. Likewise, similar support and out-of-plane conditions of the test set-up were simulated in ANSYS. The rotations about the x & y axes and the displacement in the y and z directions of the supports in the finite element model were constrained. On one side of support, the displacement in the x direction constraint was constrained which was considered as a simply support. To prevent localized distortion and avoid severe stress concentration of the elements adjacent to the supports, an additional support plate using the same solid element attaching the bottom beam flange was used accordingly. It has been turned out that this method provided a more even stress distribution on the flange surface connecting the support. In accordance with the characteristics of test load in Fig. 5, the maximum load of 80kN was applied at the centre of span in the finite element modelling to replicate the loading response of the test beam.

## 4. Stress Distribution Analysis

Von Mises yield criterion was adopted in the static finite element analysis. Table 2 lists the comparison of the results of mid-span deflection (measured by LVDTs) and strain (measured by strain gauges) obtained from experimental measurement and finite element analysis. It can be seen that the finite element analytical values are slightly higher than experimental values with the error less than 10% in this case, but this difference can be disregarded due to the initial surface condition of the flange plate in the test specimen. The stress contours resulting from finite element analysis in Fig. 9 show that in the vicinity of the centre of span, the web-to-flange fillet weld at the intersection of the longitudinal fold and the inclined fold of the corrugated web is greatly stressed. The maximum von Mises stress is 248.61 MPa, which is 55% of the material yield strength. In contrast, the stress on the corrugated web is much lower even at the centre of span which indicates that the flange plate contributes greatly to the overall bending moment. The stressed concentrated intersection in the finite element model compares well with the location where fatigue failure took place in the test, as shown in Fig. 9. This indicates that local stress concentration is significant even when the corrugated web beam meets safety requirement in the static loading condition. As mentioned earlier, the monotonic loading tests were conducted at several given intervals. Fig. 10 schematically compares the test and numerical moment-deflection response of the specimens with corrugation angles of $45^o$. It can be seen that numerical predictions agree well with the initial slopes of the test curves which confirms a good representation of the stiffness of test beams.

**Table 2** Comparison of mid-span deflection and strain results from experiment and modelling

| Measured points | Test 1 ($\alpha$=30º) | | | Test 2 ($\alpha$=45º) | | |
|---|---|---|---|---|---|---|
| | Experimental | Numerical | Error (%) | Experimental | Numerical | Error (%) |
| | Strain ($\mu\varepsilon$) | | | | | |
| a | 789.7 | 866 | 8.81 | 1119.9 | 1289 | 6.44 |
| b | 663.5 | 711 | 6.68 | 979.5 | 1038 | 5.64 |
| c | 587.7 | 623 | 5.57 | 907.5 | 967 | 6.15 |
| d | 447.1 | 469 | 4.67 | 794.5 | 843 | 5.75 |
| | Maximum defection (mm) | | | | | |
| m | 2.42 | 2.37 | 2.06 | 2.92 | 2.81 | 3.4 |

Note: the number of measured points can be referred to that SG locations illustrated in Fig.4.



[ DOI: 10.22068/IJCE.13.4.419 ]

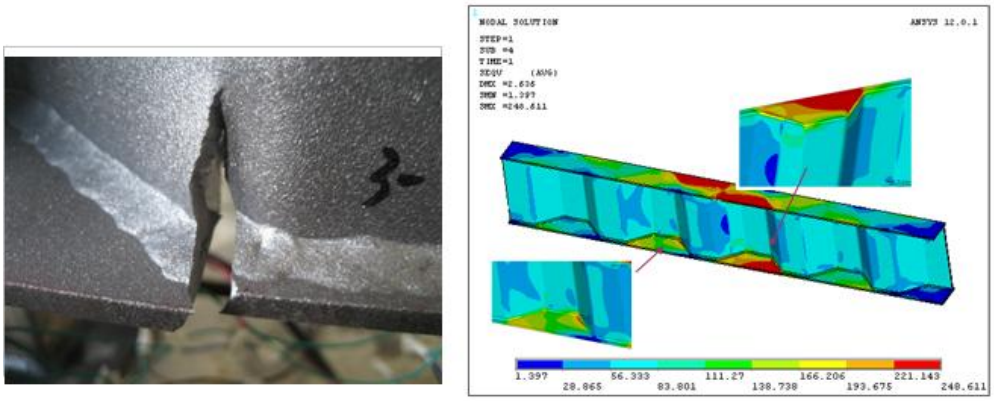

**Fig. 9** Comparison of fatigue failure location with critical stress contours in modelling ($\alpha$=45º)

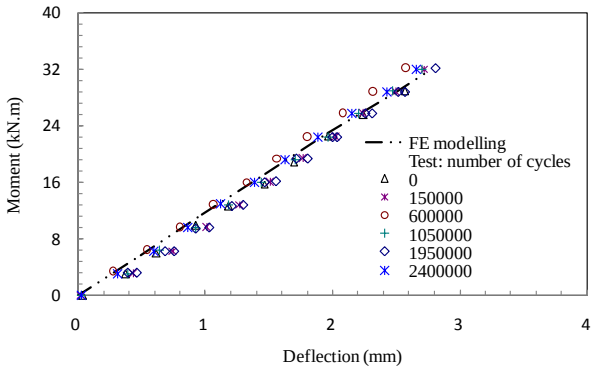


**Fig. 10** Comparison of experimental and numerical moment-deflection relations ($\alpha$=45º)

In order to further examine the failure at the web-to-flange fillet weld, two fracture surfaces between the ends of the longitudinal fold and the inclined fold of the corrugated web were analysed. On closer examination at outer location via micrographic illustration with magnification of 500, it can be observed that the fatigue crack initiated from the weld toe adjacent to the internal corner of the corrugated web and then propagated into the tension flange plate of the corrugated steel web beam, as shown in Fig. 11(a). On the other hand, the micrograph view at inner location indicates that the fatigue crack also initiates from the weld root in the vicinity of the external corner of the corrugated web, as shown in Fig. 11(b). For the purpose of visual comparison, a cutaway view at same location in the finite element model is illustrated in Fig. 12. It can be seen that the corresponding location of the weld toe and the weld root are greatly stressed. Also, the stress through plate thickness decreases gradually from the top surface of the tension flange.

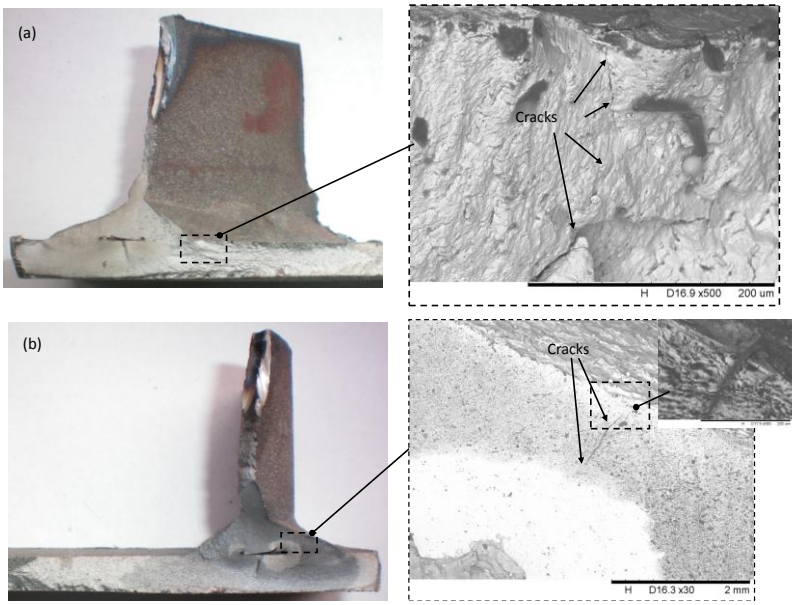


**Fig. 11** Failure surface and micrograph of the web-to-flange welded joint: (a) crack initiation from weld toe, (b) crack initiation from weld root



[ DOI: 10.22068/IJCE.13.4.419 ]

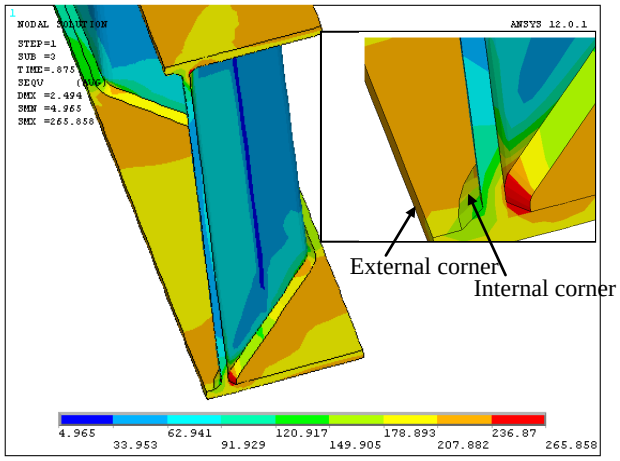


**Fig. 12** Numerical stress contours at crack initiation region

## 5. Effective Notch Stress Analysis

Since aforementioned fatigue cracks are susceptible to take place from the weld toe and the weld root, the effective notch stress approach was adopted to evaluate the web-to-flange welded joint in these critical regions. The notch stress was obtained via the finite element model with fictitious rounds with effective notch radius of 1mm in the weld toe and the weld root. This radius value has been verified to give consistent results for structural steels [15].

In the finite element model for effective notch stress analysis, the flange plate connects corrugated web by the web-to-flange fillet weld and exclusively carries longitudinal load. This model replicates the web-to-flange welded joint in the corrugated web beam in bending. The local geometry of the web-to-flange weld joint was determined from local cross-section micrograph of the beam specimen. Given that the stressed web-to-flange fillet welds at the intersection of the longitudinal fold and the inclined fold of the corrugated web are potentially subject to fatigue failure, the effective notch sections were chosen at the angles of 0º, 15º, 30º, 45º to the cross-section perpendicular to the longitudinal fold of the corrugated web as a reference section. Between the upper and lower weld root contours, the root gap of 0.5mm is introduced, as shown in Fig. 13 (a) &(b). The local parts around the weld toe and the weld root were also modelled using SOLID185 element mentioned previously in the beam model. In the vicinity of the fictitious hole corresponding to the weld toe and the weld root, the mesh was refined to allow a more accurate appraisal of the notch stress, as illustrated in Fig. 13(c). The effective notches of 1mm are included for the weld toes at the internal and external corners of the corrugated web. A tensile nominal stress of 120 MPa was applied as a pressure load at the tip surface of the flange plate.

**(a)**

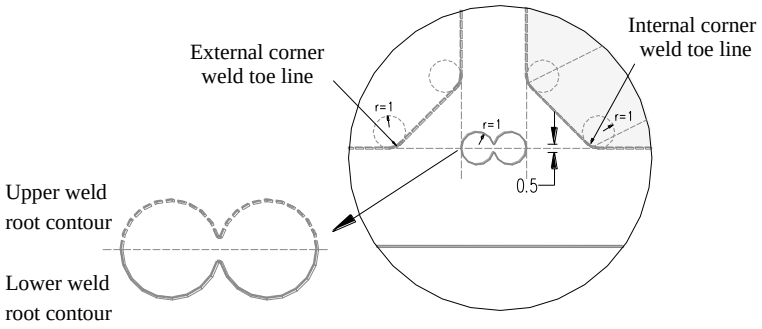


**(b)**

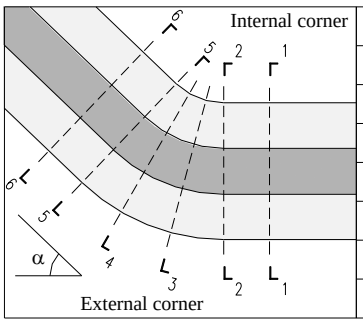


| No. | Label |
|---|---|
| 1 | 0° outside section |
| 2 | 0° section |
| 3 | 15° section |
| 4 | 30° section |
| 5 | 45° section |
| 6 | 45° outside section |
| α | corrugation angle |



[ DOI: 10.22068/IJCE.13.4.419 ]

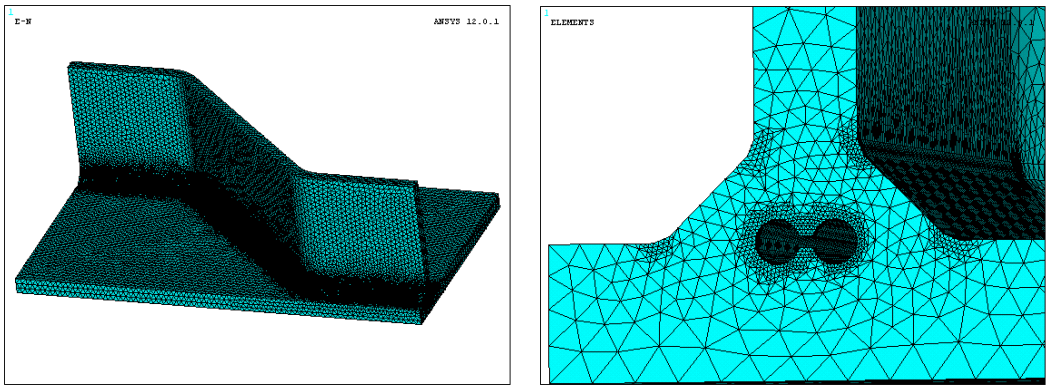


**Fig. 13** Schematic of a web-to-flange welded joint in effective notch stress analysis: (a) fictitious rounding of weld toes and roots; (b) details at the intersection of longitudinal fold and inclined fold of the corrugated web; (c) local element mesh

In the effective notch stress analysis, the principal stress and equivalent stress are normalized by the nominal stress on the flange plate. As shown in Fig. 14, regarding the notch section of the internal corner weld toe line, the magnitude of normalized principal stress is smaller than that of the normalized equivalent stress, and the reverse tends to be the case for the external corner weld toe line. In contrast, the normalized principal stress and equivalent stress are almost equivalent in the range of weld root notch. When comparing the magnitude of the notch stress of the weld toe and the weld root, the highest stress takes place at the weld toe corresponding to the internal corner of the corrugated web if the angle of the notch section is 0º~30º with respect to the reference section. The location of this highest stress corresponds well to the crack initiation point in the test specimen, as shown in Fig. 11(a). On the other hand, the weld toes at the external corner of the corrugated web exhibit the highest stress when the notch section locates between 30º and 45º, relative to the reference section, the weld toes corresponding to the external corner of the corrugated web exhibit the highest stress. The notch stress variation in the weld root range tends to be greater than that in the weld toe range, and this trend is increased with the increase of the aforementioned reference section angle. Additionally, when the reference angle is 30º, the highest notch stresses of the weld root and weld toe corresponding to the internal and external corners of the corrugated web are quite close to each other. In this case, it is expected that both the weld toe and the weld root are prone to suffer crack initiation which can be referred to the test observation in Fig. 11b. Hence, these results indicate that it is possible to expect the fatigue crack failure arising at the weld root or weld toe corresponding to the external and internal corner of the corrugated webs from the effective notch stress analysis.

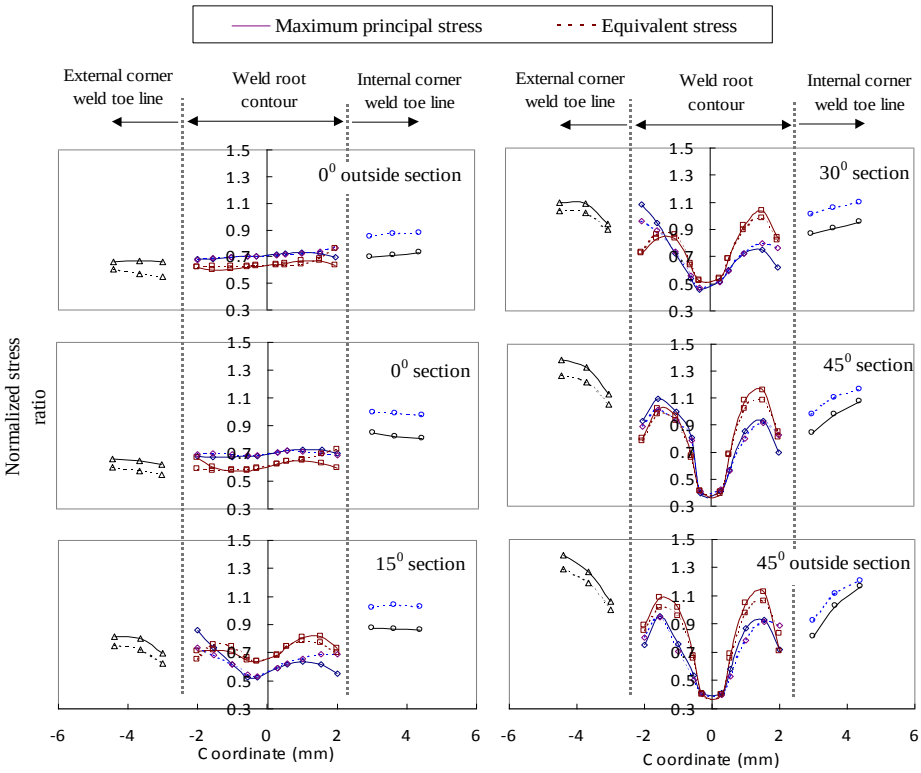


**Fig. 14** Normalized stress ratio distribution on the notch surface



[ DOI: 10.22068/IJCE.13.4.419 ]

## 6. Fatigue Life Analysis

*6.1. Finite element analytical approach*

Following foregoing finite element analysis, the dataset output file containing stresses, strains, or forces of the finite element model forms a file with an extension as '.rst' type. This file was further exported into software package FE-SAFE 6.2 for post-processing stress-life analysis. The program will then detect elements on the surface of the structural component and limit the fatigue analysis to those elements only at given loading step or increment. As a result, the number of cycles to failure and factor of safety of the corrugated steel web beam can be predicted accordingly.

The material *S-N* curve is a log scale plot of the stress amplitude versus the number of stress cycles to failure. For steels, this curve can be simplified as a slope line connecting the fatigue strength ($S_{f,0}$) at $10^3$ cycles to that at the endurance limit ($S_e$) at $10^6$ cycles and more. Based on the popular curve fits in the literature [16], an estimation of $S_f$ is given in relation to the ultimate tensile strength ($S_{ut}$) as:

$$S_{f,0} = 0.9S_{ut} \tag{3}$$

Similarly, the stress endurance limit ($S_e^{'}$) for ideal laboratory specimens can also be related to $S_{ut}$. For steels with $S_{ut}$<1460MPa, the relationship can be written as:

$$S_e^{'} = 0.504S_{ut} \tag{4}$$

To take into account the realistic condition different from the laboratory, the Marin factors[17] that qualify the effects of material, manufacturing, environment and design can be incorporated into the expression of $S_e$ as:

$$S_e = k_{sf}k_{sz}k_{ld}k_{tm}S_e^{'} \tag{5}$$

where, $k_{sf}$ is surface modification factor depending on the quality of the finish of the actual part surface and the tensile strength of the part material which can be expressed as:

$$k_{sf} = 57.7S_{ut}^{-0.718} \tag{6}$$

when the hot-rolled surface and $S_{ut}$ in MPa are considered. The calculated $k_{sf}$ is 0.618 for $S_{ut}$ =555MPa. $k_{sz}$ is the size modification factor which can be given for bending component as:

$$k_{sz} = \begin{cases} 1.24d^{-0.107} & 2.79\text{mm} \le \text{d} \le 51\text{mm} \\ 1.51d^{-0.157} & 51\text{mm} \le \text{d} \le 254\text{mm} \end{cases} \tag{7}$$

Here, $d$ is the diameter of a round bar which can be converted from a rectangular section of dimensions $b \times h$ as $d$=0.808($hb$)$^{0.5}$. The loading modification factor $k_{ld}$ is 1.0 for bending condition and the temperature modification factor $k_{tm}$ is also 1.0 for the temperature ranging between 0 °C and 250 °C.

If $S_{f,0}$ and $S_e$ are known, the approximated equation for the fatigue strength ($S_f$) between the cycle corresponding to $S_{f,0}$ and that at the endurance limit can be expressed as:

$$S_f = aN^b \tag{8}$$

where, $a$ and $b$ are constants [17] which are given as:

$$\begin{cases} a = \dfrac{(S_{f,0})^2}{S_e} \\ b = -\dfrac{1}{3}\log\left(\dfrac{S_{f,0}}{S_e}\right) \end{cases} \tag{9}$$

It is noted that the calculated fatigue strength is also influenced by the existence of structural irregularities or discontinuities which increases the local stress significantly. In this regard, a stress concentration factor (SCF) should be taken into account. For the purpose of simplicity, the SCF obtained from the static finite element analysis can be further used in the calculation of fatigue strength.

After the definition of the *S-N* relation and its corresponding modification factors, the fatigue algorithm is chosen for each element or node group based on the material properties in FE-SAFE. To take into account the effect of varying midrange (mean) stress ($S_m$) and stress amplitude ($S_a$), the fatigue failure criteria is used for the correction of calculated $S_e$. The Gerber failure criterion, which can be expressed in the following equation, was adopted in this analysis.

$$\frac{S_a}{S_e} + \left(\frac{S_m}{S_{ut}}\right)^2 = 1 \tag{10}$$

This is due to the consideration that: when plotted in the Haigh diagram (indicating $S_m$- $S_a$ relation), the nonlinear parabola relationship formed by eq.10 has better results of passing among the midrange tension data and permitting quantification of the probability of failure in contrast to the straight line by the Goodman criterion [18]. Also, the Gerber failure criterion is well suitable for the structural steel as a ductile material used for corrugated web beam. The calculation of $S_m$ and $S_a$ can be given as:

$$\begin{cases} S_m = \dfrac{\sigma_{\max} + \sigma_{\min}}{2} \\ S_a = \dfrac{\sigma_{\max} - \sigma_{\min}}{2} \end{cases} \tag{11}$$

It is noted that $\sigma_{min}$ and $\sigma_{max}$ are the stresses corresponding to the minimum (8kN) and maximum (80kN) applied loads respectively. Given the longitudinal flexibility of the corrugated web is greater with respect to the flange plate, the overall bending moment is assumed to be carried primarily by the longitudinal flange plate. In this regard, the minimum and maximum stresses on the top surface of the bottom flange can be calculated as 12.92MPa and 129.28MPa respectively.



[ DOI: 10.22068/IJCE.13.4.419 ]

Numerical fatigue life contours for the corrugated web beam plotted as $\log_{10}$ of fatigue life are depicted in Fig. 15. It is shown that the worst-case life of the model locating at the centre of span in the vicinity of the intersection of the longitudinal fold and the inclined fold of the corrugated web. This region almost coincides with the stress concentration regions in the stress analysis. Also, it can be seen that the worst-case life region on the flange plates covers a spreading area along the web-to-flange fillet weld connecting the inclined fold of the corrugated web. This observation agrees with the crack initiation at this location in the fatigue test as indicated in Fig.6(a). The fatigue lives in terms of cycles can be further obtained by an exponential function base 10 expression in converting. Hence, the estimated failure lives are in the range of 2773320 to 3162278 load cycles, which indicate slightly underestimated (with corresponding error range between 13.3% and 1.2%) but on the safe side with respect to the number of cycles to failure in the fatigue test.

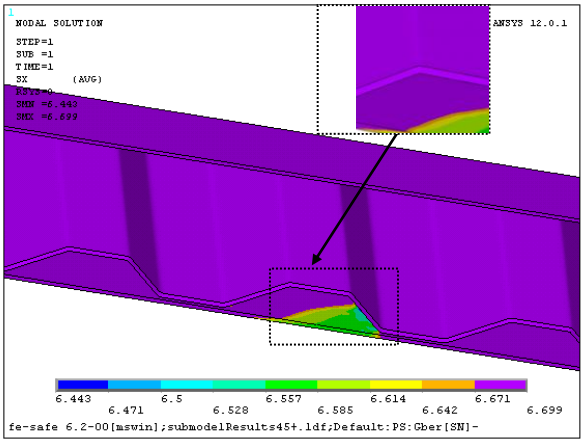


**Fig. 15** Fatigue life estimation for the crack initiation region plotted as $\log_{10}$ of fatigue life

For the fatigue limit design, the factor of strength (FOS) describing the fatigue life of materials within a function of working stress was performed in this study. In the Haigh diagram, the FOS indicates that how much the stress could be increased from the origin until the mean stress relationship curve could be reached. The FOS analysis process is repeated until it exceeds the maximum factor (default 2.0) or is less than the minimum factor (default 0.5) [19]. The contours of stress based safety factor distribution are shown in Fig. 16. The minimum safety factor is 0.969 at the intersection of the longitudinal fold and the inclined fold of the corrugated web on the bottom flange plate. From this point, the distributing of low safety factor between 0.969 and 1.198 can be seen in this region with fold line boundary near the centre of span. Again, this corresponds well to the stress concentration induced fatigue crack and failure observed in the test. The accuracy of the fatigue life predicted by finite element modelling was further verified by comparing the life predictions with the experimental results reported by Sause et al. [6] and Korashy et al. [15]. As shown in Fig. 16, the good correlation between the predictions and experimental data for different specimens and stress ranges indicates the confidence of using finite element analysis in the fatigue life assessment of the corrugated web beams.

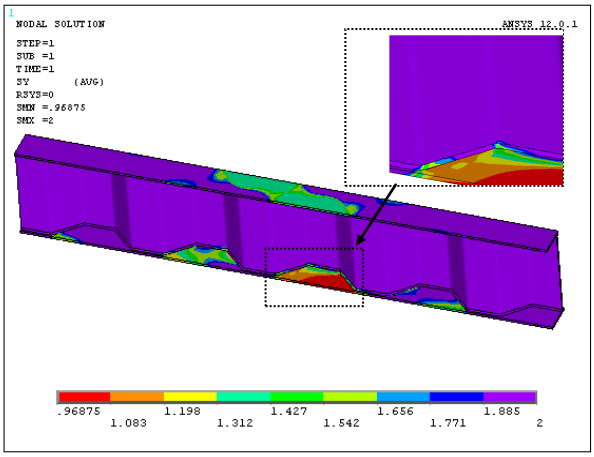


**Fig. 16** Numerical safety factor contour of the corrugated web beam

*6.2. Fracture mechanics approach*

Based on the experimental observation, the fatigue failure initiated at the welds intersected with the corrugated web and the flange plate. The linear elastic fracture mechanics was also adopted in this study for the fatigue life prediction accordingly. It was assumed that the fatigue crack grew at the weld toes which can be modelled as a semi-elliptical surface crack into the flange plate [22,23]. The stress intensity factor $\Delta K$ can be defined as:

$$\Delta K = F_S F_E F_T F_G \Delta\sigma \sqrt{\pi a} \tag{12}$$

where, $F_S$ is a free surface correction factor, $F_E$ is a crack shape correction factor, $F_T$ is a finite thickness correction factor, $F_G$ is a geometry correction factor, $\Delta\sigma$ is an applied stress range, and $a$ is a crack depth. Each correction factor can be obtained from expressions as follows.

$$F_S = 1.211 - 0.186\sqrt{\frac{a}{c}} \tag{13}$$

$$F_E = \frac{1}{E(k)} \tag{14}$$

$$E(k) = \int_0^{\frac{\pi}{2}} \left[1 - \left(1 - \frac{a^2}{c^2}\right)\sin^2\theta\right]^{0.5} d\theta \tag{15}$$

$$F_T = 1.0 \tag{16}$$

$$F_G = \frac{K_t}{1 + 0.88a^{0.576}} \tag{17}$$

The initial crack size is denoted as $a_i$ and the final crack size, $a_f$, is equal to the thickness of the flange plate. The major to minor axis semi-elliptic edge crack shape ratio $c/a$ can be taken as 1.33 and kept constant. $K_t$ is the maximum stress concentration factor at the weld toe which was obtained from aforementioned finite element analysis.



[ DOI: 10.22068/IJCE.13.4.419 ]

The number of cycles required to propagate the initial crack through the flange plate was estimated by the Paris law based integrating expression, as follows:

$$N = \frac{1}{C}\int_{a_i}^{a_f} \frac{1}{\Delta K^m} da \tag{18}$$

where, the coefficient of $C$ is a constant value which can be obtained from classic metal fatigue test. As for the steel material in this study, the value of $9.694\times10^{-10}$ $mm^{5.5}/N^2$ was adopted as suggested by Barsom and Rolfe [21]. When plotted on log-log scales, the relationship between alternating stress and number of cycles to failure can be described by a straight line with the slope of $m$. Based on the fatigue test results, a constant value of $m$=3 has been used for fatigue detail categories in the design code [22,24]. Substituting eq. (12) into eq. (18) and using logarithmic transformation, the fatigue life estimation can be obtained.

For further comparison with aforementioned numerical results and experimental data reported in [6] and [15], the fatigue life required to propagate through the flange plate thickness is written in SI units as:

$$\log N = 12.69 - 3\log(\Delta S) \tag{19}$$

As shown in Fig. 17, the slope representing eq.(19) is in very close agreement with the numerical result which indicates a slightly underestimated but on the safe side prediction of the fatigue life of the corrugated web beam. For detailed studies, the fracture mechanics life predictions along with the numerical results and experimental data are summarized in Table 3. In design specifications, the relation between the stress range, $\Delta S$, and the number of cycles, $N$, has the form [22]:

$$N = A(\Delta S)^m \tag{20}$$

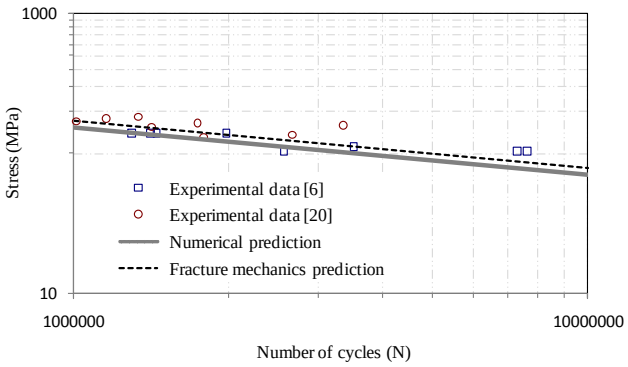


**Fig. 17** Comparison of numerical predicted fatigue lives with experimental results reported in the literature

where $A$ is a proportionality coefficient dependent on details. Using log-log transformation, the fatigue test data can be related for comparison. The number of cycles corresponding to each detail category can be calculated provided that $\Delta S$ and $A$ are known. Based on the original fatigue resistance of detail categories and related log$A$ values defined in the AASHTO fatigue design code [24], the life results mentioned above are also compared in logarithm with their counterpart corresponding to fatigue categories. It can be seen in Table 3 that the numerical and fracture mechanics life results for most prediction lie between AASHTO fatigue categories $B$ and $B$' and correlate reasonably well with the test results.

**Table 3** Comparison of test and predicted log($N$) with AASHTO fatigue categories

| | Stress level log ($S$) (MPa) | Number of cycles, log ($N$) | | | | | |
|---|---|---|---|---|---|---|---|
| | | Test | Numerical | Fracture mechanics | AASHTO fatigue categories | | |
| | | | | | B | B' | C |
| Current tests | 2.17 | 6.52 | 6.51 | 6.48 | 6.09 | 5.80 | 5.65 |
| | 2.07 | 6.51 | 6.44 | 6.45 | 6.37 | 6.08 | 5.92 |
| Sause et al.[6] | 2.14 | 6.15 | 6.13 | 6.27 | 6.17 | 5.88 | 5.73 |
| | 2.01 | 6.41 | 6.51 | 6.65 | 6.56 | 6.26 | 6.11 |
| | 2.14 | 6.30 | 6.13 | 6.27 | 6.17 | 5.88 | 5.73 |
| | 2.04 | 6.54 | 6.43 | 6.57 | 6.47 | 6.18 | 6.02 |
| Korashy et al.[20] | 2.30 | 5.90 | 5.66 | 5.80 | 5.70 | 5.41 | 5.26 |
| | 2.25 | 6.07 | 5.81 | 5.95 | 5.85 | 5.56 | 5.41 |
| | 2.19 | 6.15 | 5.97 | 6.11 | 6.02 | 5.72 | 5.57 |
| | 2.14 | 6.43 | 6.14 | 6.28 | 6.19 | 5.89 | 5.74 |
| | 2.12 | 6.25 | 6.19 | 6.33 | 6.23 | 5.94 | 5.78 |
| | 2.27 | 6.13 | 5.75 | 5.89 | 5.80 | 5.50 | 5.35 |
| | 2.23 | 6.01 | 5.85 | 5.99 | 5.89 | 5.60 | 5.44 |
| | 2.21 | 6.24 | 5.91 | 6.05 | 5.96 | 5.66 | 5.51 |

*6.3. Parameter variation analysis and discussion*

For the purpose of enhancing the fatigue life of the corrugated web beam, it is necessary to decrease the premature failure before the fatigue life has been exhausted by improving surface condition and reducing



[ DOI: 10.22068/IJCE.13.4.419 ]

stress concentration. It is known that the surface finish is a stress dependent property, and can be used to incorporate other stress dependent phenomena. Also, the material fatigue strength is greatly influenced by the fatigue failure nucleating at the plate surface. Therefore, a comparative analysis was first made by varying the surface finish factor at the centre of span of the model where fatigue vulnerability occurs. In FE-SAFE, the default surface finish factor for mirror polished component is 1.0 and can be modified no less than 1.0 for other surface types. In this sense, the predefined surface finish factor is imported as the reciprocal of aforementioned $k_{sf}$. As shown in Fig. 18, the structural fatigue life is increased with the increase of $k_{sf}$ from 0.568 to 0.645 which apparently indicates that the surface finish effect near the weld jointing the inclined fold of the corrugated web close to the centre of span affects the fatigue life of the corrugated web beam.

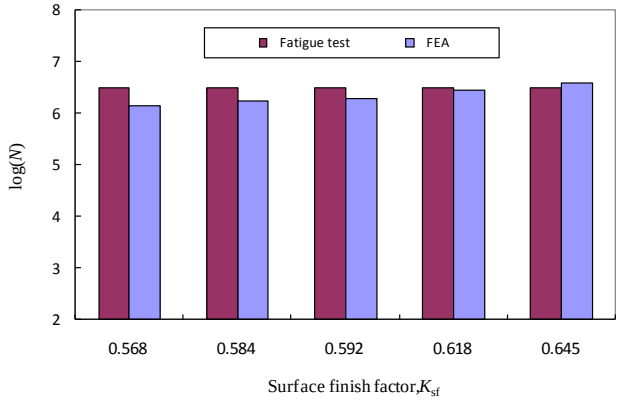


**Fig. 18** Comparison of experimental and numerical fatigue life with varying $K_{sf}$ ($\alpha$=45º)

In structural design, the flange thickness, $t_f$, and the corrugation angle, $\alpha$, are determined as the geometric configuration parameters and their influences on the fatigue life are considered. As compared in Fig. 19, it can be seen that the structural fatigue life is gradually increased from $10^{6.32}$=2089296 cycles to $10^{6.689}$=4886524 cycles with the increase of flange thickness from 5mm to 10mm. This is due to the fact that, for the beams with identical depth, the thicker flange plates tend to have lower stress which in turn lessens the crack propagation at the weld toe in contrast to thinner flange plates. Notwithstanding that, it must be pointed out that the increase of flange thickness inevitably causes significant weight increase, e.g., the structural weight per unit length (kg/m) along the longitudinal direction of the corrugated steel web beam is increased by 17% with the increase of flange thickness from 6mm to 8mm. As an alternative solution, the corrugated web beam may be redesigned by decreasing the corrugation angle. From the viewpoint of the configuration, this can avoid or reduce an abrupt change of stress state at the end of the inclined fold intersecting with the longitudinal fold of corrugated web. For this comparison, the aforementioned finite element analysis was repeated for the corrugation beam with the corrugation angle of 30º and the corresponding result is depicted in Fig. 19. It can be seen that this decrease of corrugation angle obviously amplifies the fatigue life of the corrugated beam by 34.6% which is roughly comparable to the increase of flange thickness of 2mm, i.e. from $t_f$=6mm to $t_f$=8mm. In this regard, if the shear strength requirement of the corrugated web is satisfied, it is possible to enhance the fatigue life of the corrugated web beams under critical stress state by decreasing the corrugation angle or smoothing the intersecting geometry of the longitudinal fold and the inclined fold of the corrugated web. Additionally, the increase of the flange thickness within appropriate range may also be applied as a supplement for such consideration.

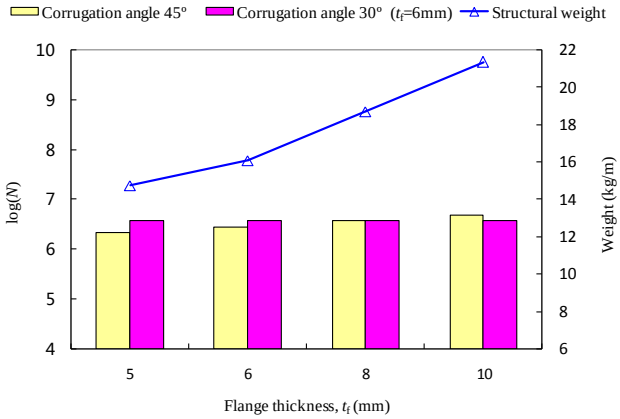


**Fig. 19** Comparison of fatigue life estimation as a function of tf and weight

## 7. Summary and Conclusion

Based on a general fatigue analytical procedure, the finite element based fatigue assessment of corrugated steel web beams was performed in this study. The analysed specimen is configurationally comparable to the component of interest in the highway bridges. The stress concentration in the vicinity of the web-to-flange welded joint at the intersection of the longitudinal fold and the inclined fold of the corrugated web was identified in the modelling. The notable stressed region and deformation related variables in the finite element modelling compared well with the experimental results.

The web-to-flange welded joint corresponding to the critical region in the test beam was analysed based on the effective notch stress approach. The principal stress and equivalent stress are almost equivalent in the range of weld root with respect to those of the weld toe. On the effective notch sections with angles at 0º~30º and 30º~45º to the reference section, the highest notch stresses occur at the weld toes corresponding to the internal and external corners of the corrugated web respectively. When the reference angle is 30º, the highest notch stresses at the weld root and weld toe are quite close. The comparison with the fatigue test results showed that it is possible to expect the fatigue crack failure arising at the weld root or weld toe corresponding to the sections with reference angle using the effective notch stress analysis.

The numerical fatigue life analysis was carried out using the endurance limit modification factors defined material *S-N* relation and the Gerber failure criterion. Also, the fracture mechanics analysis was performed in the


[ DOI: 10.22068/IJCE.13.4.419 ]

prediction of fatigue life required to propagate through the thickness of the flange plate. The resultant fatigue lives of referred corrugated steel web beams are compared between AASHTO fatigue categories *B* and *B*'. The estimated *S-N* relations showed good correlation with slightly underestimated but on the safe side with respect to the fatigue test results. To improve the fatigue life of the corrugated steel web beams, a comparative study was performed taking into account the solution of improving the surface condition and reducing stress concentration of components. From a viewpoint of design, an alternative application of decreasing the corrugation angle or smoothing the intersection geometry of the corrugated web was suggested together with a moderate increase of the flange thickness within appropriate range. The analytical results justified the proposed application in the enhancement of the fatigue life of the corrugated steel web beams.

**Acknowledgements:** The research work described in this paper was supported by the National Natural Science Foundation of PR China (No. 51308363 & No. 11327801), the Scientific Research Foundation for the Returned Overseas Chinese Scholars (No. 2013-1792-9-4) and the Start-up Research Fund for Introduced Talents of Sichuan University (No. YJ201307).

## References

[1] Huang L, Hikosaka H, Komine K. Simulation of accordion effect in corrugated steel web with concrete flanges, Computers and Structures, 2004, Vol. 82, pp. 2061-2069.

[2] Innovative practice of prestressed concrete box-girder bridges with corrugated steel webs, Henan Provincial Communications Planning Survey & design Institute Co.Ltd. May, 2012 (in Chinese). <http://www.hnrbi.com/kcsjy/html/737/3373/2012-5-29/179536.html>

[3] Ma L, Jin JG, Wan S. Experimental and numerical investigation of the Weihe bridge, In: Proceedings of the 20th national conference on structural engineering, Ningbo, Zhejiang, China, 5-7 November, 2010 (in Chinese).

[4] Maddox SJ. Fatigue strength of welded structures, 2nd ed. Cambridge, England, Abington Publishing, 1991.

[5] Ibrahim SA, El-Dakhakhni WW, Elgaaly M. Behavior of bridge girders with corrugated webs under monotonic and cyclic loading, Engineering Structures, No. 28, 2006, pp. 1941-1955.

[6] Sause R, Abbas HH, Driver RG, Anami K, Fisher JW. Fatigue life of girders with trapezoidal corrugated webs, Journal of Structural Engineering, ASCE, 2006, No. 7, Vol. 132, pp. 1070-8.

[7] Li G, Luo X, Sun F, Fan X. Experimental investigation on fatigue performance of welded H-beam with corrugated webs, Journal of Building Structures, No. 1, 2012, pp. 96-103 (in Chinese).

[8] Kövesdi B, Dunai L. Fatigue life of girders with trapezoidally corrugated webs: An experimental study, International Journal of Fatigue, 2014, No. 64, pp. 22-32.

[9] Wang ZY, Tan LF, Wang QY. Fatigue strength evaluation of welded structural details in corrugated steel web girders, International Journal of Steel Structures, No. 13, 2013, pp. 707-721.

[10] Wang ZY, Wang QY. Fatigue assessment of welds joining corrugated steel webs to flange plates, Engineering Structures, No. 73, 2014, pp. 1-12.

[11] Wang ZY, Wang QY. Fatigue strength of CFRP strengthened welded joints with corrugated steel plates, Composites: Part B, 2015(72): 30-39. .

[12] Takesita A, Yoda T, Sato K, Sakurada M. Fatigue tests of a composite girder with corrugated web, Proceedings of annual conference of the Japan society of civil engineering, No. 52, 1997, pp. 122-123 (in Japanese).

[13] GB50017-2003. Code for design of steel structures, Beijing, China Planning Press (in Chinese), 2003.

[14] GB/T8110-2008. Welding electrodes and rods for gas shielding arc welding of carbon and low alloy steel, Beijing, Standardization Administration of China (SAC) (in Chinese), 2009.

[15] Hobbacher A, editor. Recommendations for fatigue design of welded joints and components. IIW-Document XIII-2151-07/XV-1254-07. Update May 2003, Paris, France, InternationaI Institute of Welding, 2003.

[16] Charles RM. Prediction of stochastic endurance strength. Trans. of ASME, Journal of Vibration, Acoustics, Stress, and Reliability in Design, 1987, No. 1, Vol. 109, pp. 113-122.

[17] Shigley JE, Mischke CR. Mechanical Engineering Design, McGraw-Hill, Inc, NewYork, 1989.

[18] Collins JA. Failure of Materials in Mechanical Design, Analysis, Prediction, Prevention, John Wiley & Sons, 1993.

[19] Fatigue theory reference manual. Safe Technology Limited, 2002, No. 1, Vol. 2.

[20] Korashy M, Varga J. Comparative evaluation of fatigue strength of beams with web plate stiffened in the traditional way and by corrugation, Acta Tech. Acad. Sci. Hung, 1979, No. 89, pp. 309-346.

[21] Barsom JW, Rolfe ST. Fracture and fatigue control in structures, 3rd Ed, ASTM, Butterworth-Heinemann, 1999.

[22] Hirt MA, Fisher JW. Fatigue crack growth in welded beams, Engineering Fracture Mechanics, 1973, No. 5, 415-429.

[23] Broek D. Elementary engineering fracture mechanics, Kluwer Academic Publishers, 2nd ed, 1986.

[24] AASHTO. AASHTO LRFD bridge design specifications, 3rd Ed, AASHTO, Washington, D.C, 2004.



[ DOI: 10.22068/IJCE.13.4.419 ]